23rd ABCM International Congress of Mechanical Engineering
December 6-11, 2015, Rio de Janeiro, RJ, Brazil

FREQUENCY ESTIMATION OF BACKWARD-WHIRL DURING ROTOR-STATOR CONTACT

Benjamin Siegl
Oliver Alber
Richard Markert
Institute of Structural Dynamics, TU Darmstadt
siegl@sdy.tu-darmstadt.de
alber@sdy.tu-darmstadt.de
markert@sdy.tu-darmstadt.de

Abstract. *This paper deals with an analytical estimation for the negative frequency components which can be detected during rotor-stator contact for a motion pattern called backward-whirl. If this backward-whirl occurs depends on the parameter set of the rotor, stator and contact area. But if it takes place usually the amplitudes become very high and severe damage might be caused to the system. As a conclusion this motion pattern should be avoided during operation. The presented method is based on previous research which estimated the backward-whirl frequency of a Laval rotor in contact with a stator with one degree of freedom. This paper extends this method for rotors with multi-degrees of freedom (MDOF) contacting MDOF stators. A phenomenon which is characteristic for such systems is the transition from a backward-whirl motion pattern to another one with potentially even higher amplitudes.*

Typically, the gap between rotor and stator is very small compared to the backward-whirl amplitudes. Because of this, the negative backward-whirl frequency component for each chosen rotor speed is very close to a negative natural frequency of the coupled rotor-stator system. Thus, this coupled natural frequency can be used for a bi-frequent approach to solve the equations of motion. This gives rise to the calculation of the resulting backward-whirl amplitudes for a MDOF rotor at each rotor speed.

Keywords: *Rotor dynamics, Rotor-stator contact, Backward-Whirl*

LIST OF SYMBOLS

A	center of the contact ring
$\boldsymbol{B}$	damping matrix
b	damping coefficient, N s/m, N m s
D	damping ratio
$\boldsymbol{f}$	excitation force vector
F	force, N
$\boldsymbol{G}$	gyroscopic matrix
i	complex unit
$\boldsymbol{K}$	stiffness matrix
k	stiffness coefficient, N/m, N, N m
$\boldsymbol{l}$	position vector for contact-DOF
M	mass center of the disk
$\boldsymbol{M}$	mass matrix
m	mass, kg
R	shaft center
r	complex displacement, m
$\boldsymbol{r}$	displacement vector
S	center of the stator
s	average nominal gap, m
y	horizontal axis
z	vertical axis

Greek Symbols

β	angular eccentricity of the disk
δ	instantaneous minimal gap, m
ε	radial eccentricity, m
$\boldsymbol{\varepsilon}$	eccentricity vector, m
Θ	moment of inertia, kg m^2
μ	friction coefficient
Ω	rotor speed, Hz
ω	natural frequency, Hz
φ	rotation angle of the rotor
Ψ	asynchronous whirl frequency, Hz
ψ	contact point angle

Operators

$\arg\{\square\}$	argument
$\mathrm{diag}\{\square\}$	diagonal matrix
$\widehat{\square}$	amplitude
$\square^T$	transposed
$\dot{\square}$	$\dfrac{\mathrm{d}}{\mathrm{d}t}$

Subscripts

A	contact ring
a	axial
b	backward
C	contact
f	forward
M	center of mass, number of stator-DOF
N	normal, number of rotor-DOF
n	n-th
p	polar
R	rotor
RS	rotor and stator rigidly coupled
S	stator
T	tangential
φ	rotation

1. INTRODUCTION

When a rotor contacts a non-rotating part (so-called *stator)*, which can e. g. be its housing or an auxiliary bearing, the whole dynamic system becomes nonlinear and various motion patterns may occur. Some of these motions, e. g. synchronous, forward whirl, sideband, sub-, superharmonic and chaotic motion patterns, exhibit a dominant synchronous frequency component. Furthermore, backward-whirl motion patterns are possible. In literature the backward-whirl is also often called *dry whip* (Childs and Bhattacharya, 2007). This motion pattern generally contains a small synchronous frequency component as well as a dominant negative asynchronous frequency component. It exhibits large vibration amplitudes combined with huge contact forces which might lead to severe damage of the whole rotor-stator system.

In the case of a simple LAVAL rotor (also known as JEFFCOTT rotor) contacting a flexibly mounted rigid stator Black (1968) described the possible backward-whirl motion pattern with a harmonic approach only containing an asynchronous frequency component Ψ. The rotor and stator deflections (r_R, r_S) as well as the contact force F_C are expressed by

$$r_R(t) = \widehat{r}_R e^{i\,\Psi t}, \qquad r_S(t) = \widehat{r}_S e^{i\,\Psi t} \qquad \text{and} \qquad F_C(t) = \widehat{F}_C e^{i\,\Psi t}. \tag{1}$$

This approach is widely known in literature and has been used in many further investigations, e. g. by Bartha (2000) and Crandall (1990). Lingener (1990) performed experimental studies confirming these theoretical assumptions. Ehehalt *et al.* (2004) took into account an additional small synchronous frequency component to describe backward-whirl motion. This approach is more general than Equation (1). Childs and Bhattacharya (2007) extended the simple model and investigated backward-whirl motion with a multimode rotor and a single-mode stator model. It was concluded that for multimode rotor-stator contact many backward-whirl motions are possible. Multiple coexisting backward-whirl motions have also already been identified experimentally (Wilkes *et al.*, 2010). For a slightly different model considering a LAVAL rotor with an additional degree of freedom for the inclination angle and therefore significant gyroscopic effects Siegl *et al.* (2013) also showed the occurrence of multiple backward-whirl motions. Semi-analytical approaches have been developed by Norrick *et al.* (2013) for rotors with distinctive gyroscopic effects and by Alber *et al.* (2013) for rotor-stator systems with many degrees of freedom.

2. MODELING ASSUMPTIONS

For the following investigations multiple degrees of freedom of the rotor are accomplished by using the two rotor models shown in Figure 1. The *first* rotor model (Figure 1, left) consists of a massless flexible shaft (stiffness matrix $\boldsymbol{K}_R$) carrying a rigid disk (mass matrix $\boldsymbol{M}_R$, radial mass eccentricity ε_M, angular eccentricity β) which is externally damped (damping matrix $\boldsymbol{B}_R$). The gyroscopic effect is included in the gyroscopic matrix $\boldsymbol{G}_R$ and requires an additional degree of freedom for the tilting of the disk (Gasch *et al.*, 2006). The *second* rotor model (Figure 1, right) has N disks with negligible gyroscopic effects. Every disk can have a complex eccentricity ε_{Mn}, noted in the eccentricity vector $\boldsymbol{\varepsilon}_M$. Both rotor models can be described by the general equation

$$\boldsymbol{M}_R\,\ddot{\boldsymbol{r}}_R + (\boldsymbol{B}_R+\boldsymbol{G}_R)\,\dot{\boldsymbol{r}}_R + \boldsymbol{K}_R\,\boldsymbol{r}_R = \boldsymbol{M}_R\,\boldsymbol{\varepsilon}_M\,\Omega^2\,e^{i\,\Omega t} - \boldsymbol{l}_R\,F_C \tag{2}$$

with the contact forces $-\boldsymbol{l}_R F_C$.

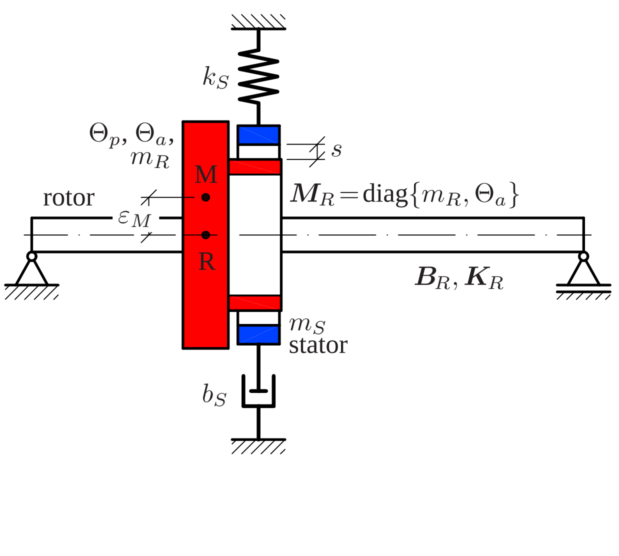

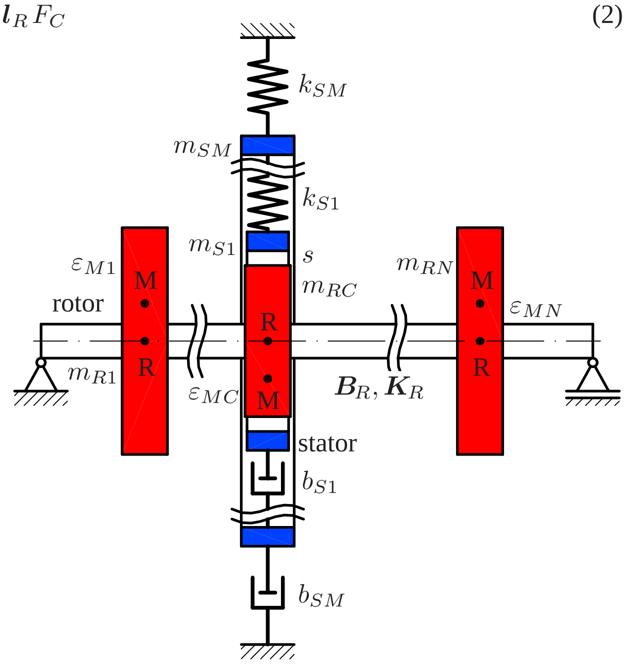

Figure 1. Rotor models with gyroscopics (Siegl *et al.*, 2013) and multi-mode rotor-stator systems (Alber, 2012).

The rotor contacts the stator at position C with cylindrical contact surfaces at an average distance s. The stator system may consist of M flexibly mounted rigid bodies with an isotropic stiffness matrix $\boldsymbol{K}_S$:

$$\boldsymbol{M}_S\,\ddot{\boldsymbol{r}}_S + \boldsymbol{B}_S\,\dot{\boldsymbol{r}}_S + \boldsymbol{K}_S\,\boldsymbol{r}_S = \boldsymbol{l}_S\,F_C. \tag{3}$$

The contacting coordinates for the rotor and the stator are described by the contact position vectors $\boldsymbol{l}_R$ and $\boldsymbol{l}_S$, which contain the value one for the contacting coordinates and otherwise zero. If the rotor and the stator are moving independently from each other or if contact is established is determined by the instantaneous minimal gap δ between rotor and stator. The kinematic equation for this instantaneous minimal gap can be set up with Figure 2:

$$\boldsymbol{l}_R^T\boldsymbol{r}_R - \boldsymbol{l}_S^T\boldsymbol{r}_S + \varepsilon_A\,e^{i\,\Omega t} = (s-\delta)\,e^{i\,\psi}. \tag{4}$$

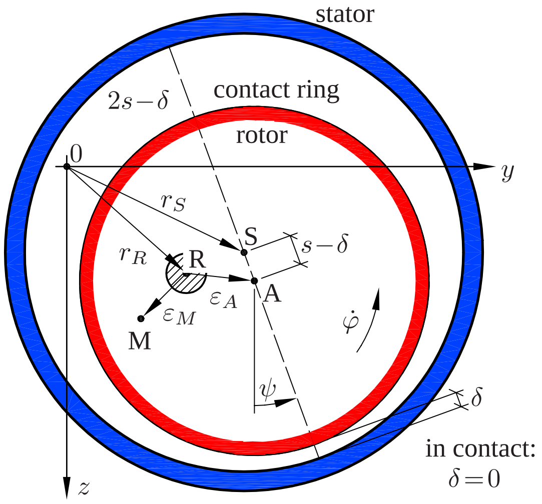

Figure 2. Kinematics in the contact plane (Ehehalt *et al.*, 2004).

Contact is established if the instantaneous minimal gap δ is smaller or equal to zero. Then, a nonlinear contact force F_C appears, which is composed of a normal component F_{CN} and a tangential component F_{CT}. Assuming COULOMB's friction law with the friction coefficient μ, the contact force is given by

$$F_C = (1 + i\,\mu)\,F_{CN} \tag{5}$$

as long as the relative circumferential velocity between rotor and stator at the contact point C is positive. The contact angle

$$\psi = \arg\left\{\boldsymbol{l}_R^T\boldsymbol{r}_R - \boldsymbol{l}_S^T\boldsymbol{r}_S + \varepsilon_A\,e^{i\,\Omega t}\right\} \tag{6}$$

and the minimal gap function

$$\delta = s - (\boldsymbol{l}_R^T\boldsymbol{r}_R - \boldsymbol{l}_S^T\boldsymbol{r}_S + \varepsilon_A\,e^{i\,\Omega t})\,e^{-i\,\psi} \tag{7}$$

can be obtained from the kinematic relation in Equation (4). In case of no contact ψ defines the direction of smallest distance δ; and in case of contact ψ defines the direction of the normal component of F_C:

$$e^{i\psi} = \frac{\boldsymbol{l}_R^T\boldsymbol{r}_R - \boldsymbol{l}_S^T\boldsymbol{r}_S + \varepsilon_A\,e^{i\,\Omega t}}{|\boldsymbol{l}_R^T\boldsymbol{r}_R - \boldsymbol{l}_S^T\boldsymbol{r}_S + \varepsilon_A\,e^{i\,\Omega t}|} = \frac{F_{CN}}{|F_{CN}|} = \frac{1 - i\,\mu}{\sqrt{1+\mu^2}}\,\frac{F_C}{|F_C|} \tag{8}$$

Several contact models are discussed in Markert and Wegener (1998). It is shown that as long as appropriate contact parameters are chosen, the type of contact model has no significant effect on the calculated global behavior of rotor stator systems. In this paper two contact descriptions are used: The kinematic condition $\delta = 0$ for continuous contact is resulting in

$$\boldsymbol{l}_R^T\boldsymbol{r}_R - \boldsymbol{l}_S^T\boldsymbol{r}_S + \varepsilon_A\,e^{i\,\Omega t} = s\,\frac{1 - i\,\mu}{\sqrt{1+\mu^2}}\,\frac{F_C}{|F_C|}. \tag{9}$$

This relation is based upon rigid contact surfaces. For contact the degrees of freedom are reduced by one. This equation is primarily used for analytical investigations. For numerical simulations the pseudolinear contact model by Ehehalt *et al.* (2004)

$$F_C = (1 + i\,\mu)\,F_{CN} = (1 + i\,\mu)\left\langle k_C\,(-\delta) - \langle b_C\,\dot{\delta}\rangle\right\rangle\langle -\delta\,\rangle^0\,e^{i\,\psi}, \tag{10}$$

is more suitable, where

$$\langle\delta\rangle^n = \begin{cases} 0 & \text{when} \quad \delta \le 0 \\ \delta^n & \phantom{\text{when}} \quad \delta > 0 \end{cases} \tag{11}$$

is an extended switching function (also called FÖPPL symbol). This model avoids tensile forces as well as discontinuities in the contact force. For sufficient contact stiffness k_C the model delivers similar results as the kinematic contact model from Equation (9).

The contact models from Equations (9) and (10) are only valid if the rotor and the stator are sliding on each other, so the constraint for COULOMB's friction law is not violated — the relative tangential velocity between rotor and stator is greater than zero. If the shaft center of the rotor is propagating backwards with a constant frequency Ψ, the condition for sliding

$$\dot{\Psi} < -\Omega\,\frac{d_R}{2\,s} \tag{12}$$

results (Bartha, 2000). According to Ehehalt (2008), in most systems the average nominal gap s is small compared to the rotor diameter at the contact point d_R, so the condition in Equation (12) is violated only for very small rotation speeds Ω. Nevertheless, a widely used definition for *backward-whirl* motion is a rotor rolling in the stator which can only occur if the kinematic boundary condition for rolling is valid. That would lead to a backward roll frequency Ψ_{roll} proportional to the rotating speed Ω (Bartha, 2000)

$$\Psi_{roll} = -\Omega\,\frac{d_R}{s}. \tag{13}$$

Lingener (1990) and Wilkes *et al.* (2010) experimentally observed sliding of the rotor in the stator. The case of rolling is not studied in this work.

3. ANALYTICAL APPROXIMATE APPROACH FOR BACKWARD-WHIRL

The equations of motion for the rotor (2) and the stator (3) with multiple degrees of freedom as well as the kinematic contact condition in Equation (9) can be analyzed with respect to possible backward-whirl motions patterns. As shown in many publications, e. g. (Ehehalt *et al.*, 2004) and (Wilkes *et al.*, 2010), the frequency spectrum of a backward-whirl motion pattern with continuous contact between rotor and stator generally exhibits a synchronous frequency component Ω as well as a negative asynchronous frequency component Ψ. Therefore a multifrequent approach similar to Ehehalt *et al.* (2004)

$$\boldsymbol{r}_R(t) = \widehat{\boldsymbol{r}}_{R\Omega}\,e^{i\,\Omega t} + \widehat{\boldsymbol{r}}_{R\Psi}\,e^{i\,\Psi t} \tag{14}$$

$$\boldsymbol{r}_S(t) = \widehat{\boldsymbol{r}}_{S\Omega}\,e^{i\,\Omega t} + \widehat{\boldsymbol{r}}_{S\Psi}\,e^{i\,\Psi t} \tag{15}$$

$$F_C(t) = \widehat{F}_{C\Omega}\,e^{i\,\Omega t} + \widehat{F}_{C\Psi}\,e^{i\,\Psi t} \tag{16}$$

for the rotor deflections $\boldsymbol{r}_R$, the stator deflections $\boldsymbol{r}_S$ and the contact force F_C is used. Separation of the frequency components results in a set of equations for the synchronous frequency Ω

$$[\boldsymbol{K}_R - \Omega^2\,\boldsymbol{M}_R + i\Omega\,(\boldsymbol{B}_R + \boldsymbol{G}_R)]\,\widehat{\boldsymbol{r}}_{R\Omega} = \Omega^2\,\boldsymbol{M}_R\,\boldsymbol{\varepsilon}_S - \boldsymbol{l}_R\,\widehat{F}_{C\Omega} \tag{17}$$

$$[\boldsymbol{K}_S - \Omega^2\,\boldsymbol{M}_S + i\Omega\,\boldsymbol{B}_S]\,\widehat{\boldsymbol{r}}_{S\Omega} = \boldsymbol{l}_S\,\widehat{F}_{C\Omega} \tag{18}$$

as well as a set of equations for the asynchronous frequency Ψ

$$[\boldsymbol{K}_R - \Psi^2\,\boldsymbol{M}_R + i\Psi\,(\boldsymbol{B}_R + \boldsymbol{G}_R)]\,\widehat{\boldsymbol{r}}_{R\Psi} = -\boldsymbol{l}_R\,\widehat{F}_{C\Psi} \tag{19}$$

$$[\boldsymbol{K}_S - \Psi^2\,\boldsymbol{M}_S + i\Psi\,\boldsymbol{B}_S]\,\widehat{\boldsymbol{r}}_{S\Psi} = \boldsymbol{l}_S\,\widehat{F}_{C\Psi} \tag{20}$$

According to Ehehalt (2008) during backward-whirl the asynchronous frequency components are much bigger than the synchronous ones, $|\widehat{F}_{C\Psi}| \gg |\widehat{F}_{C\Omega}|$. With this postulation $|F_{C\Omega} + F_{C\Psi}|$ can be replaced by $|F_{C\Psi}|$ in the kinematic relation (9). Furthermore, the eccentricity of the contact ring ε_A is neglected. This yields

$$(\boldsymbol{l}_R^T\,\widehat{\boldsymbol{r}}_{R\Omega} - \boldsymbol{l}_S^T\,\widehat{\boldsymbol{r}}_{S\Omega}) = s\,\frac{1 - i\mu}{\sqrt{1+\mu^2}}\,\frac{\widehat{F}_{C\Omega}}{|\widehat{F}_{C\Psi}|} \tag{21}$$

for the synchronous frequency Ω and

$$(\boldsymbol{l}_R^T \widehat{\boldsymbol{r}}_{R\Psi} - \boldsymbol{l}_S^T \widehat{\boldsymbol{r}}_{S\Psi}) = s \frac{1-i\mu}{\sqrt{1+\mu^2}} \frac{\widehat{F}_{C\Psi}}{|\widehat{F}_{C\Psi}|} \tag{22}$$

for the asynchronous frequency Ψ. Solving for the dominant asynchronous frequency component, inserting $\widehat{\boldsymbol{r}}_{R\Psi}$ and $\widehat{\boldsymbol{r}}_{S\Psi}$ from Equations (19) and (20) into Equation (22) for the contact force the expression

$$|\widehat{F}_{C\Psi}| = -s \frac{1-i\,\mu}{\sqrt{1+\mu^2}} \frac{1}{\boldsymbol{l}_R^T [\boldsymbol{K}_R - \Psi^2 \boldsymbol{M}_R + i\Psi\,(\boldsymbol{B}_R + \boldsymbol{G}_R)]^{-1} \boldsymbol{l}_R + \boldsymbol{l}_S^T [\boldsymbol{K}_S - \Psi^2 \boldsymbol{M}_S + i\Psi\, \boldsymbol{B}_S]^{-1} \boldsymbol{l}_S} \tag{23}$$

can be obtained. With the side condition that the amplitude $|\widehat{F}_{C\Psi}|$ has to be real,

$$\Im\{|\widehat{F}_{C\Psi}|\} \stackrel{!}{=} 0, \tag{24}$$

the unknown asynchronous frequency Ψ can be calculated using Equation (23). From now on it is treated as a known parameter. The right hand side of Equation (23) contains the complex transfer functions at the contact point of the rotor and the stator

$$H_{RCC}(\Psi) = \boldsymbol{l}_R^T [\boldsymbol{K}_R - \Psi^2 \boldsymbol{M}_R + i\Psi\,(\boldsymbol{B}_R + \boldsymbol{G}_R)]^{-1} \boldsymbol{l}_R \tag{25}$$

$$H_{SCC}(\Psi) = \boldsymbol{l}_S^T [\boldsymbol{K}_S - \Psi^2 \boldsymbol{M}_S + i\Psi\, \boldsymbol{B}_S]^{-1} \boldsymbol{l}_S \tag{26}$$

which can be used to transform Equation (23) to

$$[H_{RCC}(\Psi) + H_{SCC}(\Psi)]|\widehat{F}_{C\Psi}| = -s \frac{1-i\,\mu}{\sqrt{1+\mu^2}}. \tag{27}$$

The amplitudes of the asynchronous rotor and stator deflections $\widehat{\boldsymbol{r}}_{R\Psi}$ and $\widehat{\boldsymbol{r}}_{S\Psi}$ can be calculated using Equations (19) and (20). Combining (17), (18) and (21) the synchronous contact force component can be expressed by

$$\widehat{F}_{C\Omega} = \frac{\boldsymbol{l}_R^T [\boldsymbol{K}_R - \Omega^2 \boldsymbol{M}_R + i\Omega\,(\boldsymbol{B}_R + \boldsymbol{G}_R)]^{-1} \Omega^2 \boldsymbol{M}_R \boldsymbol{\varepsilon}_S}{s \dfrac{1-i\mu}{\sqrt{1+\mu^2}} \dfrac{1}{|\widehat{F}_{C\Psi}|} + \boldsymbol{l}_R^T [\boldsymbol{K}_R - \Omega^2 \boldsymbol{M}_R + i\Omega\,(\boldsymbol{B}_R + \boldsymbol{G}_R)]^{-1} \boldsymbol{l}_R + \boldsymbol{l}_S^T (\boldsymbol{K}_S - \Omega^2 \boldsymbol{M}_S + i\Omega\, \boldsymbol{B}_S)^{-1} \boldsymbol{l}_S}. \tag{28}$$

For valid solutions the calculated asynchronous frequencies and the resulting parameters $|\widehat{F}_{C\Psi}|$, $\widehat{\boldsymbol{r}}_{R\Psi}$ and $\widehat{\boldsymbol{r}}_{S\Psi}$ have to fulfill the following side conditions:

1. $\Im\{\Psi\} \stackrel{!}{=} 0$: Whirl-frequencies have to be real.
2. $|\widehat{F}_{C\Psi}(\Psi)| > 0$: The contact force is always positive (no tensile forces).
3. $|\widehat{F}_{C\Psi}(\Psi)| \gg |\widehat{F}_{C\Omega}|$: Check backwards the postulation made to obtain Equations (21) and (22).
4. $|r_{R\Psi}| > s$: The rotor deflection must be bigger than the gap size.

4. PREDICTION OF BACKWARD-WHIRL FREQUENCIES

The analytical solution of Equation (24) is impossible for large systems because the left-hand side of Equations (19) and (20) have to be inverted. This easily leads to polynomials in Ψ of the order much bigger than 4. Such polynomials have no analytical solution (Bronstein *et al.*, 2000). So Equation (24) is solved numerically with MATLAB©.

The four above mentioned side conditions exclude most of the potential backward-whirl frequencies resulting from Equation (24). For the rotor with distinctive gyroscopic effects (primarily called "first rotor", Figure 1 left) in Figures 3 (left) and 3 (right) the remaining frequencies are printed as the solid black lines. They are close to the backward coupled natural frequencies of the rotor-stator system. Additionally, they match the backward-whirl frequencies obtained by numerical simulations in the time domain of the rotor in contact (blue). Furthermore, the existence of two different backward-whirl frequencies and the fact that there is a transition from one backward-whirl motion pattern to another can be predicted (Figure 3, right). In both Plots in Fig. 3 (left) and 3 (right) are dash-dotted lines. The dash-dotted green lines show the speed-dependent natural frequencies $\omega_{nf/b}$ of the rotor whitout contact. The dash-dotted lines represent the natural frequencies $\omega_{RS,nf/b}$ of the coupled rotor-stator system as if it had no initial gap s. The solid grey lines are the synchronous Ω and the asymptotic $\Theta_p/\Theta_a\,\Omega$ for the second forward natural frequency ω_{2f} of a single-disk rotor with distinctive gyroscopics.

Figure 3 (left) is a CAMPBELL diagram for a slow run-up with a certain rotor-stator configuration which is defined by Ehehalt *et al.* (2005) and Ehehalt (2008) as a "light stator". This means that the first natural frequency of the coupled rotor-stator system in contact reaches resonance in the same frequency band as the stator without contact. For this specific parameter set, synchronous resonance occurs at about $\Omega = 46.6$ Hz due to unbalance excitation. Below the synchronous resonance speed, the rotor-stator system moves in a backward-whirl motion as shown by Siegl *et al.* (2013). The negative frequency corresponding to the backward-whirl obtained by the numerical simulation is displayed in Figure 3 (left) as a blue line. The darker the blue line, the higher the amplitudes of the rotor. Obviously, this frequency component is very close to the first negative natural frequency of the coupled system $\omega_{RS,1b}$ but in the frequency band between the coupled and the uncoupled natural frequency (marked yellow). The black solid line represents the backward-whirl frequency component predicted by the analytical method shown in this paper. One can see that it is very close to the results of the numerical simulation. In the numerical study, backward-whirl exists for higher rotor speeds than the analytical results predict.

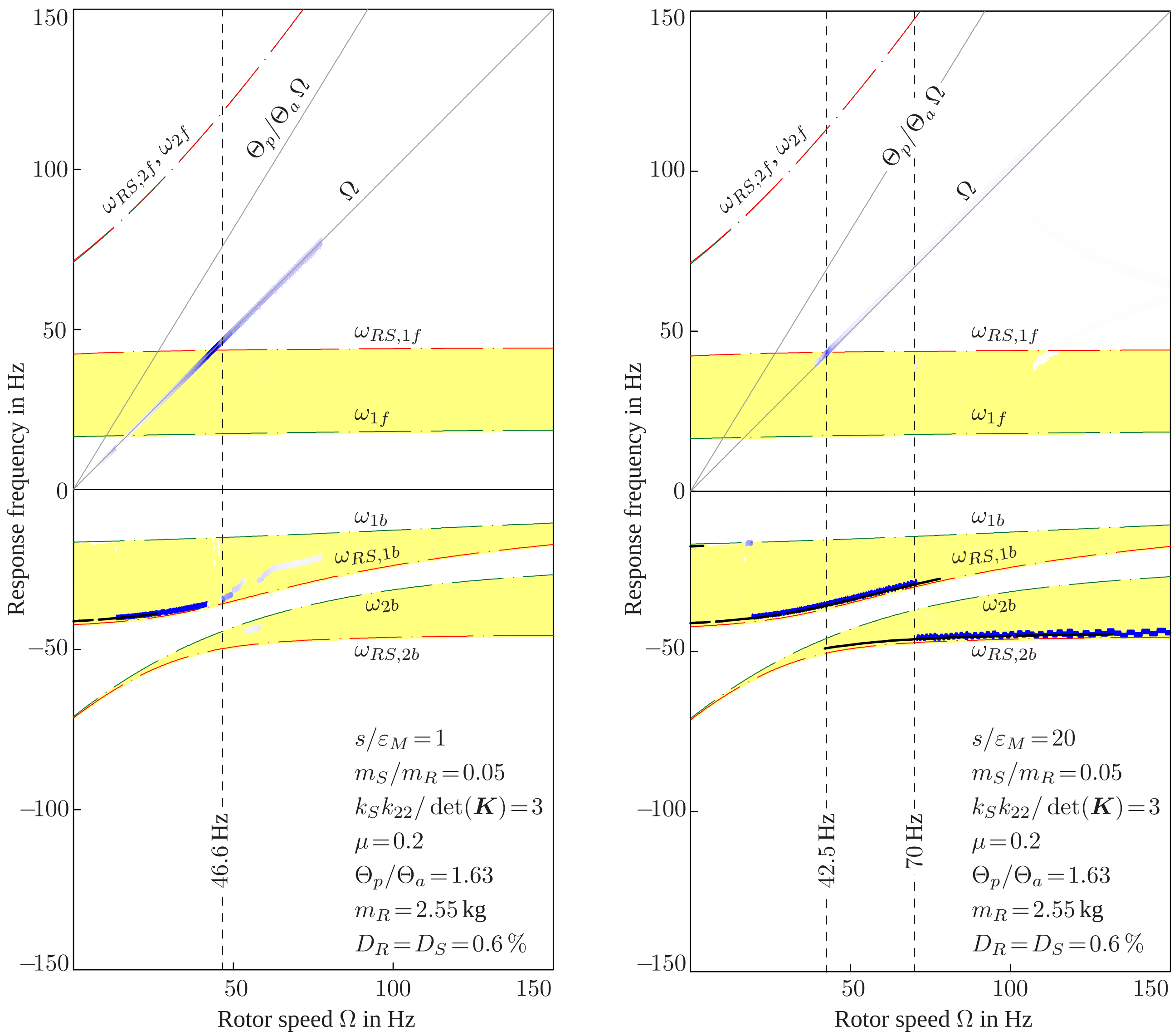

Figure 3. CAMPBELL diagrams for the rotor with distinctice gyroscopic effects; left: narrow gap, right: wide gap.

Even more impressive is the result for the "very light" stator (Figure 3, right) created by changing the width of the gap to $s/\varepsilon_M = 20$ and otherwise using the same parameters. This configuration is characterized by a natural frequency of the stator that is higher than the natural frequency of the coupled system. Here, according to the numerical simulation, synchronous resonance occurs at about $\Omega = 42.5$ Hz, again for the system in contact showing a distinctive backward whirl. At a rotor speed of about $\Omega = 70$ Hz the motion pattern jumps to another backward-whirl motion pattern with a different negative frequency component. As in the first example, both negative frequency components are close to the respective backward natural frequencies of the coupled system and in the area between those and the respective uncoupled natural frequencies of the rotor. The whirl frequencies predicted by the method shown in this paper are apparent as black solid lines. They are very close to the results of the numerical simulation and coexist in the rotor speed range from 42.5 Hz to above 70 Hz. In this rotor speed range, the transition from one backward-whirl motion pattern to another is possible. A sharp criterion for the point of transition is not evident.

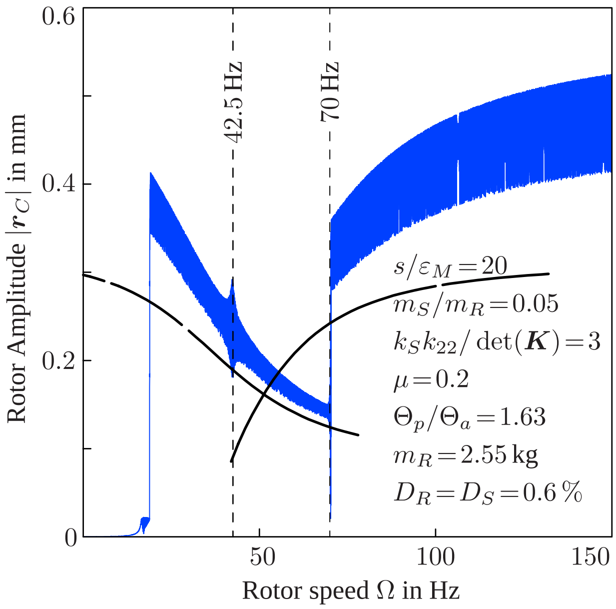

Figure 4. Rotor amplitudes for the rotor-stator configuration with wide gap $s/\varepsilon_M = 20$.

The valid solutions for Ψ are used to calculate the rotor amplitudes $|\hat{r}_{R\Psi}|$ expected during backward-whirl. Figure 4 shows a comparison of the numerical and analytical results for the second parameter set in the first rotor configuration. The blue curves are the results of the numerically simulated run-up of the rotor. The resonance peak is visible at 42.5 Hz as well as the large amplitudes due to backward-whirl in the whole rotor speed range from about 20 Hz to 150 Hz. The thick black lines are the amplitude predictions obtained from the analytical approximation. The predicted amplitudes are smaller than the amplitudes obtained numerically. This can be attributed to the neglecting of the synchronous motion due to unbalance excitation throughout the whole rotor speed range. The general shape of the rotor amplitudes during the run-up is predicted nicely.

The CAMPBELL diagrams in Figure 5 show simulations for a rotor-stator system with two degrees of freedom each and identical system parameters. On the right side different initial conditions are used for the simulation than on the left side and this leads to the occurrence of a different backward-whirl motion.

Again, the existence of two backward-whirl motion patterns can be shown, but in this case it is observed that both backward-whirl motions exist in the same rotor speed range and can be triggered by using appropriate initial conditions. As the system parameters are not speed-dependent, also the asynchronous frequencies Ψ_i do not change with the rotor speed. Furthermore, no transition between these backward-whirl motions can be observed. The analytical predictions of the whirl frequencies (solid black lines) again show a very good agreement with the simulated backward-whirl frequencies. The backward-whirl motion with $\Psi_1 = -9.47$ Hz is unstable, as it is not possible to obtain this backward-whirl motion when using the corresponding initial conditions. The other backward-whirl frequencies Ψ_2 and Ψ_3 are located next to backward coupled natural frequencies. Nevertheless, in this case the asynchronous frequency Ψ_3 differs clearly from the corresponding natural frequency $-\omega_{RS,3}$.

In Figure 6 the amplitudes of the contacting rotor disk are displayed, containing the two backward-whirl motions with the frequencies shown in Figure 5. The envelopes of these amplitudes (solid, black) can be calculated with the presented method. They approximately fit to the simulated amplitudes (blue) and again are estimated a little bit lower than the amplitudes resulting from the numerical simulation. Regarding the maximum amplitudes, the backward-whirl motion with $\Psi_2 = -12.9$ Hz is the most critical motion. The maximum amplitude of the backward-whirl motion with Ψ_3 is significantly lower. Again it has to be mentioned that the motion with Ψ_1 is not obtained in the simulation and therefore not stable.

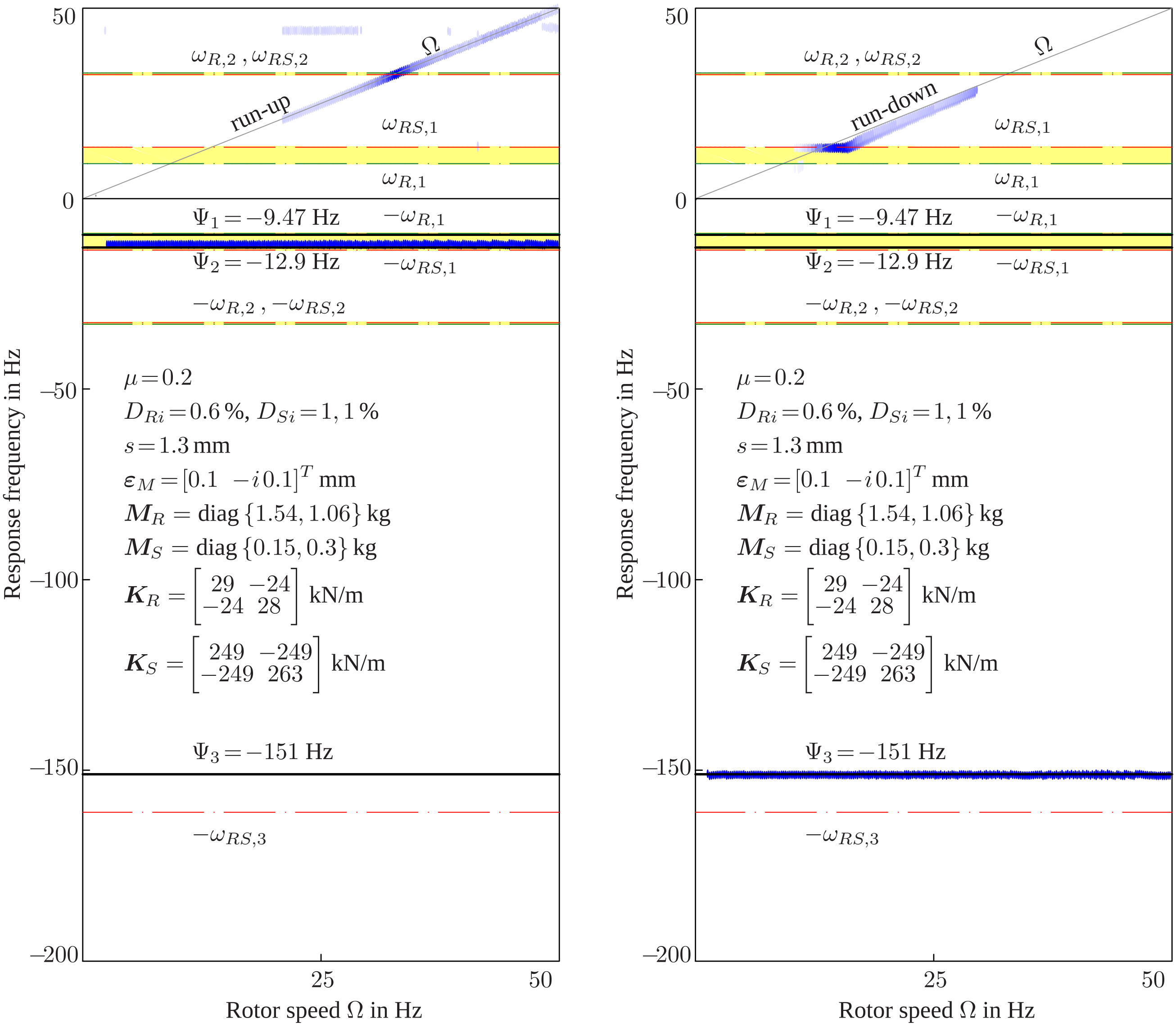

Figure 5. CAMPBELL diagrams for the same MDOF rotor-stator system; two different backward-whirl motions induced by a run-up and a run-down.

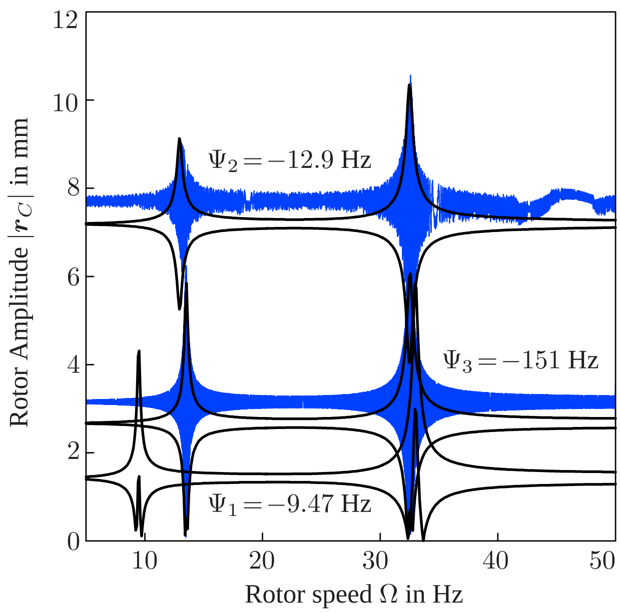

Figure 6. Rotor amplitudes of the contacting disk for the multi-disk rotor-stator configuration of Figure 5.

5. CONCLUSIONS

The method explained in this paper allows the prediction of backward-whirl motion patterns, frequencies and amplitudes for rotor-stator contact of rotor-stator systems with multiple degrees of freedom. The determination or at least the estimation of the dominant asynchronous frequency is of great advantage, as it is the dominant excitation frequency for both rotor and stator system during backward whirl. The knowledge allows for the design of rotor-stator systems which are able to outwear load cases of a backward whirl during operation of the machine.

The method has been demonstrated with the examples of a single-disk rotor with distinctive gyroscopic effects and a multi-disk rotor contacting a multi-body stator. The results for the negative frequency components match the results of numerical simulations made in previous papers (Siegl *et al.*, 2013; Alber *et al.*, 2013; Norrick *et al.*, 2013). Frequency areas for the appearance of transitions between motion patterns can be derived. A comparison between the results of a numerical simulation and the developed semi-analytic approach was drawn. Looking at the rotor amplitudes expected during backward-whirl it is obvious that a reliable amplitude prognosis can only be obtained by numerical simulation of the rotor-stator system.

6. REFERENCES

Alber, O., 2012. “Rotor Stator Interaction with Many Degrees of Freedom”. In *Proc. Appl. Meth. Mech.* Darmstadt, Germany, Vol. 12, pp. 251–252.

Alber, O., Norrick, N. and Siegl, B., 2013. “Multimode Backward Whirl Motion in Rotor-Stator Contact”. In *11th International Conference on Vibration Problems*. Lisbon, Portugal.

Bartha, A., 2000. *Dry Friction Backward Whirl of Rotors*. Ph.D. thesis, Swiss Federal Institute of Technology, Zürich, Switzerland.

Black, H.F., 1968. “Interaction of a whirling rotor with a vibrating stator across a clearance annulus”. *Archive: Journal of Mechanical Engineering Science 1959-1982 (vols 1-23)*, Vol. 10, No. 1, pp. 1–12.

Bronstein, I.N., Semendjajew, K.A., Musiol, G. and Mühlig, H., 2000. *Taschenbuch der Mathematik*. Harri Deutsch, Thun. ISBN 9783817120055.

Childs, D. and Bhattacharya, A., 2007. “Prediction of Dry-Friction Whirl and Whip Between a Rotor and a Stator”. *Journal of Vibration and Acoustics*, Vol. 129, No. 3, pp. 355–362.

Crandall, S., 1990. “From Whirl to Whip in Rotordynamics”. In *3rd Int. Conf. for Rotordynamics*. Lyon, France, pp. 19–26.

Ehehalt, U., 2008. *Bewegungsformen elastischer Rotoren bei Statorkontakt*. Ph.D. thesis, TU Darmstadt, Darmstadt, Germany.

Ehehalt, U., Hahn, E. and Markert, R., 2005. “Motion patterns at rotor stator contact”. In *Proc. of ASME International Design Engineering Technical Conferences and Computers and Information in Engineering Conference*. Long Beach, California, pp. 1031–1042.

Ehehalt, U., Hochlenert, D. and Markert, R., 2004. “An Analytical Description of Backward Whirl Caused by Rotor-Stator-Contact”. In *10th International Symposium on Transport Phenomena and Dynamics of Rotating Machinery*. Honolulu, Hawaii, pp. 1–10.

Gasch, R., Nordmann, R. and Pfützner, H., 2006. *Rotordynamik*. Springer, Berlin, 2nd edition. ISBN 3-540-41240-9.

Lingener, A., 1990. “Experimental Investigation of Reverse Whirl of a Flexible Rotor”. In *3rd Int. Conf. for Rotordynamics*. Lyon, France, pp. 13–18.

Markert, R. and Wegener, G., 1998. “Transient Vibrations of Elastic Rotors in Retainer Bearings”. In *7th International Symposium on Transport Phenomena and Dynamics of Rotating Machinery*. Honolulu, Hawaii, Vol. 2, pp. 764–774.

Norrick, N., Siegl, B. and Alber, O., 2013. “Backward Whirl During Rotor-Stator Contact of Gyroscopic Rotors”. In *11th International Conference on Vibration Problems*. Lisbon, Portugal.

Siegl, B., Norrick, N. and Markert, R., 2013. “Theoretical Investigations on Rotor-Stator-Contact of Rotors with Distinctive Gyroscopic Effects”. In *XV. International Symposium on Dynamic Problems of Mechanics*. Buzios, Brazil, pp. 1–9.

Wilkes, J.C., Childs, D., Dyck, B.J. and Phillips, S.G., 2010. “The Numerical and Experimental Characteristics of Multimode Dry-Friction Whip and Whirl”. *Journal of Engineering for Gas Turbines and Power*, Vol. 132, No. 5.

7. RESPONSIBILITY NOTICE